Antimicrobial and Aging Properties of Ag-, Ag/Cu-, and Ag Cluster-Doped Amorphous Carbon Coatings Produced by Magnetron Sputtering for Space Applications

Giuseppe Sanzone, Susan Field, David Lee, Jingzhou Liu, Pengfei Ju, Minshi Wang, Parnia Navabpour, Hailin Sun, Jinlong Yin,* and Peter Lievens

Cite This: https://doi.org/10.1021/acsami.2c00263

Read Online
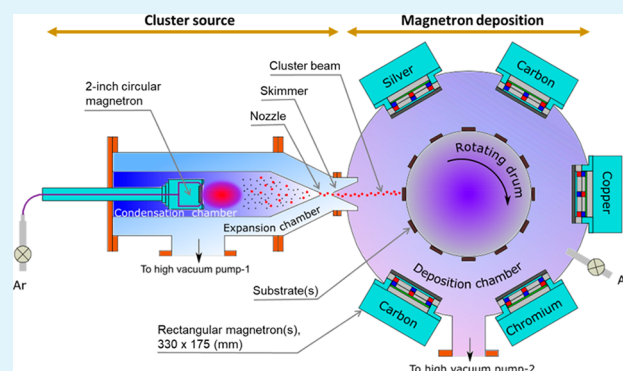
ACCESS | 📊 Metrics & More | 📖 Article Recommendations | SI Supporting Information

ABSTRACT: Inside a spacecraft, the temperature and humidity, suitable for the human crew onboard, also creates an ideal breeding environment for the proliferation of bacteria and fungi; this can present a hazard to human health and create issues for the safe running of equipment. To address this issue, wear-resistant antimicrobial thin films prepared by magnetron sputtering were developed, with the aim to coat key internal components within spacecrafts. Silver and copper are among the most studied active bactericidal materials, thus this work investigated the antibacterial properties of amorphous carbon coatings, doped with either silver, silver and copper, or with silver clusters. The longevity of these antimicrobial coatings, which is heavily influenced by metal diffusion within the coating, was also investigated. With a conventional approach, amorphous carbon coatings were prepared by cosputtering, to generate coatings that contained a range of silver and copper concentrations. In addition, coatings containing silver clusters were prepared using a separate cluster source to better control the metal particle size distribution in the amorphous carbon matrix. The particle size distributions were characterized by grazing-incidence small-angle X-ray scattering (GISAXS). Antibacterial tests were performed under both terrestrial gravity and microgravity conditions, to simulate the condition in space. Results show that although silver-doped coatings possess extremely high levels of antimicrobial activity, silver cluster-doped coatings are equally effective, while being more long-lived, despite containing a lower absolute silver concentration.

KEYWORDS: antimicrobial, clusters, nanoparticles, silver, copper, amorphous carbon, microgravity, aging, nanowhiskers

1. INTRODUCTION

A manned space station not only creates a suitable environment for its astronauts' long-term presence but also provides favorable conditions for the breeding of microorganisms.[1] The growth of bacteria and fungi is not only hazardous for the astronauts living in the space station but also responsible for equipment failure.[2] Microbial control has become an important task in the engineering design of space stations, and a source of continuous work for their long-term operation.

Between 2016 and 2018, NASA ran two projects in sequence, Microbial Tracking-1 (MT-1) and Microbial Tracking-2, to monitor the types of microbes present on the surfaces and in the air of the International Space Station (ISS) and also to catalogue and characterize potential disease-causing microorganisms onboard. NASA's latest program, the Bacterial Adhesion and Corrosion (BAC) spaceflight experiment, launched on SpaceX-21 in December 2020, will study the effect of spaceflight on the formation of multispecies, surface-adherent bacterial communities (biofilms), and their ability to

corrode stainless steel surfaces relevant to those in the International Space Station (ISS) water system.

To combat the threats from overgrown microorganisms, the employment of chemicals and disinfectants[3] has been proposed and studied; however, the use of antimicrobial coatings to control microbiological growth in a space station has emerged as a more effective and sustainable solution. Very recently, Wang et al. published a thorough and detailed review[4] on the topic of antimicrobial surfaces for applications on confined inhabited space stations, in which a selection of commercial and developed coatings targeting space applications was summarized. It was concluded that although the

approach of organic biocompatible coatings presents fewer health issues, the durability of such coatings under operational conditions is a formidable challenge to be tackled.

In this work, magnetron sputtering technology was employed to produce antimicrobial thin films with excellent mechanical strength and long durability. The silver-containing antimicrobial coatings were designed to slow down or inhibit the growth of fungi or bacteria on the surfaces. Compared to other methods, the magnetron sputtering approach provides several competitive advantages:

(1) The ceramic (e.g., CrN, TiN, TiO$_2$ or Al$_2$O$_3$) or carbon coatings prepared by this method are highly wear-resistant and scratch-resistant with high hardness, which makes them durable and well suited for the environment in a space station, where it is almost impossible to carry out repairs or replace components.

(2) Unlike chemical disinfectants, which are typically only effective for killing a narrow range of microorganisms, the Ag nanoparticles embedded in the coatings can inhibit the growth of a very broad spectrum of microbes.

(3) It is known that only the Ag nanoparticles present at the coating surface exhibit effective antimicrobial functions but that they gradually get lost through daily wear and tear. With optimized coating design, there are abundant Ag nanoparticles embedded deep inside the coating, which work as a reservoir, by slowly diffusing to the surface and replenishing Ag particles lost over time, thus providing a very long lifetime solution for space station and manned space missions.

Although silver has a long history of being extensively studied in many forms for its antimicrobial activities (see, for example, ref [5]), the doping of Ag in a PVD (physical vapor deposition) coating for such a function has been a more recent development, which began just a little over ten years ago; examples are the antimicrobial property of the Ag-doped TiN coating reported by Kelly's group[6] and the patent on a Ag-containing metal nitride coating used for orthopedic implants.[7] As the growth of bacteria, viruses, or fungi can be effectively inhibited on the coated surface without the involvement of chemicals or radiations, the development of antimicrobial PVD coatings has attracted increasing interest. Many research groups have investigated different coating materials and a combination of them, with the aim of improving the overall coating bactericidal performance as well as understanding the bacteria killing mechanisms. The PVD antimicrobial coating normally consists of two integral parts: (i) the coating matrix, which forms the main structure of the coating and provides the desired engineering properties (e.g., mechanical and tribological properties), and (ii) the doping metal, which forms the minor part of the coating but provides the critical antimicrobial property. The metal dopant can cause protein dysfunction and loss of enzyme activity inside the bacteria cell.[8] Some of the most studied coating matrix materials include titanium dioxide,[9] titanium nitride,[6] chromium nitride,[10] zirconium nitride,[11] carbon,[12] silicon dioxide nanoparticles,[13] and zinc oxide nanoparticles,[14] while the metal dopants studied include silver,[15] copper,[16] gold,[17] palladium,[18] platinum,[19] zinc,[20] and gallium.[21]

Silver and copper are among the most popular metals used for antimicrobial applications, because of their high bactericidal performance. It has been suggested that in addition to the protein dysfunction and loss of enzyme activity, Ag can disrupt the activity of the bacterial electron transport chain, effectively inhibiting the respiratory chain and generating a redox-driven transmembrane Na$^+$ potential by translocating Na$^+$ ions, while Cu can produce membrane damage.[8]

For this reason, Ag and Cu have been widely used as dopants to enhance the coating antibacterial performance. However, when such metals are added into the coating, it has been found that they gradually migrate to the coating surface. One of the most common issues found when a metal is added to a thin film, is the appearance of metal whiskers on the surface as the coating ages.[22,23] In fact, the dopant metal atoms dispersed in the coating matrix would slowly migrate toward the surface, where they agglomerate to form bigger particles or whiskers.[24−28] This degradation process is mainly driven by the metal atom mobility inside the coating matrix and by the environment at the immediate coating surface.[25,27] Ultimately, to ensure an effective antimicrobial activity over the lifetime of the coating, it would be desirable to optimize the rate of metal migration to the surface, so that migration is not too fast, causing metal loss too quickly, or too slow to maintain the replenishment capability.

Elemental composition is not the only parameter affecting the antimicrobial activity. Recent studies on Ag and Cu nanoparticles have shown that there is a strong influence of metal particle size, shape, surface charge, and other factors on the release of metal ions. In fact, smaller metal particles would oxidize easier, releasing more metal ions which in turn increases the bactericidal effect.[29−32] Control over the deposited metal nanoparticles' size distribution can be achieved either by thermal treatment during the deposition, e.g.,[33−36] or by employing a cluster source during the deposition process.[37] In the case of the cluster source approach, metal particles are preformed in the gas phase inside the cluster source and then deposited onto the substrate along with the elements which form the coating matrix, resulting in a nanocomposite coating with metal clusters embedded within. The main advantage of using a cluster source with respect to a thermal treatment is much better control over the particle size and flux, by appropriately tuning of the gas aggregation parameters.[38,39] Other advantages include a relatively narrow cluster size distribution and the absence in the main deposition chamber of metal single atoms, which would more easily diffuse and aggregate on the coating surface. Recent studies by Cavaliere et al. demonstrated that it is possible to produce highly efficient antibacterial coatings by depositing Ag−Cu−Mg alloy clusters on the surface with good control on the stoichiometry of the multielement clusters.[40] However, a relatively low cluster deposition rate has hindered this approach to be successfully adopted for the preparation of cluster embedded coatings. Only recently, a significant improvement in the throughput of the cluster source, achieved after our theoretical systematic aerodynamic study,[41] made it possible to produce nanocomposite coatings with sufficient numbers of clusters embedded inside.

Another important factor needed to be considered for the application in a manned spacecraft is that a high level of leached heavy metals, such as Ag, in a confined environment could potentially cause health issues and induce resistance in some bacteria. Therefore, the silver loading in the coating and its ion release rate should be carefully controlled, so that only a minimal amount of silver is leached into the environment, while still maintaining a highly effective bactericidal function.

In this work, the aging and antimicrobial properties of Ag-doped, Ag−Cu-doped, and Ag-cluster-doped amorphous carbon coatings were investigated under standard terrestrial gravity as well as under a microgravity environment for aerospace applications. The amorphous carbon coating, with a high percentage of sp^2 carbon bonding, displaying high corrosion resistance, high hardness, good adhesion properties, low friction coefficient, and low electrical resistivity,[42−47] is a versatile and flexible choice for coating many different types of parts found in a space station. Ag-doped and Ag−Cu-doped samples were prepared using DC magnetron cosputtering, while the Ag-cluster-doped samples were prepared with a combined cluster source and conventional magnetron sputtering chamber. For these three types of samples, mechanical properties, particle size distribution, aging, ion release rate, and antimicrobial properties have been investigated and are reported here.

2. EXPERIMENTAL SECTION

2.1. Preparation of Ag-doped Carbon Coatings by Cosputtering. The coating samples were prepared in a high vacuum magnetron sputtering chamber, with six vacuum ports equally spaced; five ports were installed with magnetrons, and the remaining one was connected to a cluster source (Figure 1). Two magnetrons were set
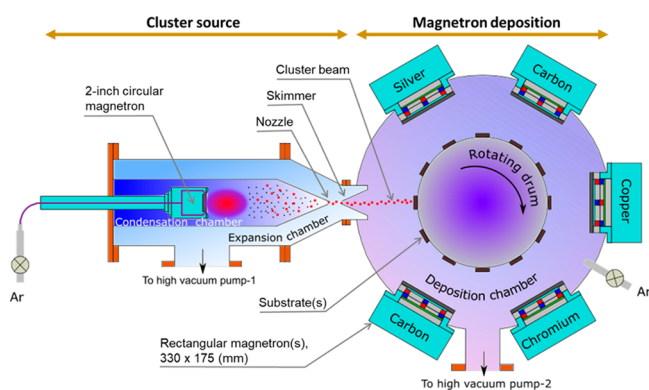

Figure 1. Schematic of the vacuum system used for the deposition of carbon thin films. The cluster source is shown on the left-hand side, while the conventional magnetron sputtering deposition chamber is shown on the right-hand side. During the cluster deposition, the pressure in the expansion chamber is controlled to be slightly higher than the pressure in the deposition chamber, so that the cluster beam can pass the skimmer without too much resistance.

up with carbon (C) targets, which were used to produce the amorphous carbon coatings. One magnetron was fitted with a chromium (Cr) target, to produce the adhesion layer between the substrate and carbon coating. The remaining two magnetrons were fitted with silver (Ag) and copper (Cu) targets, for the doping of Ag and Cu respectively into the carbon layer. Each magnetron had a rectangular shape with dimensions 330 mm × 175 mm, while the size of the targets employed in the system was 300 mm × 145 mm.

Coating substrates were 25 mm × 25 mm square, with a thickness of 1 mm. The substrate material was 304 stainless steel, and the top surface was mirror-polished. They were ultrasonically cleaned in isopropanol for 20 min prior to loading into the deposition chamber. In the chamber, the substrates were mounted on a cylindrical drum, at a distance of 150 mm from the sputtering targets. The cylindrical drum was rotating at a speed of 5 rpm during deposition to ensure a uniform coating for all of the samples loaded.

After the substrates were loaded onto the rotating drum, the vacuum chamber was pumped to a base pressure of ~5 × 10⁻⁶ mbar. Then the sputtering gas, argon (Ar) with purity of 99.99% was

admitted into the deposition chamber with a flow rate of around 20 sccm, to reach a pressure of 1.0×10^{-3} mbar. The deposition process for the amorphous carbon thin film followed the four steps below:

(i) Ion cleaning: after igniting the plasma, a pulsed bias voltage up to 500 V was applied to the substrates to etch the surface and remove any contamination.

(ii) Cr interlayer: a pure thin Cr layer was deposited first to enhance the adhesion of the coating to the substrate.

(iii) Transition layer: a transition layer was deposited next, by gradually ramping down the deposition rate of Cr, while gradually ramping up the deposition rate of carbon. At the same time "noncluster sourced" dopants were slowly introduced. As a result, the composition of this layer changed gradually from pure Cr to the composition required at step iv.

(iv) Metal-doped amorphous carbon (a-C) layer: finally the amorphous carbon layer was deposited to a thickness of 1−2 µm. By controlling the sputtering power on the carbon targets and Ag (or Cu) target, the Ag or Cu doping level in the carbon matrix was tuned.

For more detailed magnetron sputtering procedures for carbon coating deposition, please refer to previous publications elsewhere[48,49]

In step iv above, the Ag and the Cu targets were operated in power-regulated mode. Samples with different concentrations of Ag and Cu inside the carbon matrix were prepared by changing the power applied to the Ag and Cu targets, from 35 to 90 W for Ag and from 20 to 40 W for Cu.

2.2. Preparation of Ag Cluster-doped Carbon Coatings. The Ag-cluster-doped coatings were prepared with the addition of a separate cluster source. The cluster source consisted of two cylindrical chambers, one big and one small (see the left-hand side of Figure 1). The smaller chamber is referred to as the condensation chamber (also called aggregation or nucleation chamber), because it is where clusters form and grow. The bigger chamber is referred to as the expansion chamber, since it is where the gas expands and is pumped out from the system.

A 2-in. circular magnetron was used in the condensation chamber to sputter out Ag atoms under a pressure of ~1 mbar, which was about 1000 times higher than the sputtering pressure in the main deposition chamber. The high pressure helps to thermalize the sputtered atoms and increase the probability of Ag−Ag−Ar three body collisions. The three-body collision is responsible for the formation of dimers, which then grow into bigger particles by subsequent collisions with other particles.[50,51] The size distribution of clusters produced using this method is typically very narrow compared to other synthesis methods.[52] The size distribution and cluster flux can be tuned by changing synthesis parameters, e.g., power applied to the magnetron, gas flow rate, types of gas used, temperature, pressure and the residence time in the condensation chamber, which is controlled by the distance between magnetron and nozzle, i.e., the aggregation length.[38,39]

The carrier gas Ar (also acting as the sputtering gas for the circular magnetron) was injected through the 2-in. circular sputtering device, to give a much higher cluster production efficiency, compared to other gas inlet positions.[41] The Ar gas promotes the Ag sputtering process and the subsequent cluster formation process and, then, carries the clusters going through the 5 mm nozzle and enters the expansion chamber. The majority of the Ar gas is pumped out of the system by a high vacuum turbomolecular pump attached to the expansion chamber, while a small amount of Ar is leaked into the deposition chamber via the skimmer. Because of the small size of the nozzle, the Ar gas chokes at the nozzle when it rushes out of the condensation chamber, which creates a pressure barrier. As a result, the pressure inside the condensation chamber is ~2−3 orders of magnitude higher than that of the expansion chamber.[53] Clusters formed inside the condensation chamber are dragged out through the nozzle by the carrier gas in a supersonic expansion jet, in which clusters tend to stay in the center of the jet beam, while less massive particles, such as single atoms and the carrier gas, diverge radially. The skimmer, a conical orifice, with the apex facing the nozzle of the

condensation chamber, is placed downstream to extract the central portion of the supersonic expansion, so that clusters will travel further downstream ballistically into the main deposition chamber. To measure the cluster mass flux, a retractable quartz crystal microbalance (QCM) was placed in the main deposition chamber at a distance of 100 mm from the skimmer.

On the magnetron in the cluster source, a circular Ag target with a diameter of 50 mm and a purity of 99.99% was used. The magnetron was run in power-controlled mode, and a power of 80 W was applied for cluster deposition. The Ar gas flow was set at 160 sccm. The condensation chamber was cylindrical with an internal diameter of 100 mm and was provided with a conical nozzle with an apex angle of 60°. This optimized geometrical chamber configuration has been shown to increase the total cluster throughput by nearly 1 order of magnitude.[41] The cluster mass flux measured with the quartz crystal microbalance (QCM) in the deposition chamber, under these conditions, was typically 1 μg cm^{-2} s^{-1}.

Samples with Ag-clusters embedded in the carbon were prepared by following the standard four-step procedure detailed in section 2.1, then adding one more step at the end. In the fifth and final step, the power applied to the carbon targets was reduced from 8.5 to 2.3 mA cm^{-2}, while the Ag magnetron in the cluster source was turned on. The purpose of reducing the carbon deposition rate was to match it with the relatively slow Ag-cluster deposition rate. Although many new approaches have been implemented in the cluster source to improve the cluster throughput,[54] the deposition rate of Ag-clusters was still a lot lower than the deposition rate of Ag atoms sputtered from the rectangular magnetron in the deposition chamber. This additional step lasted for 30 min. Three Ag-cluster embedded carbon samples were prepared using different aggregation length: 200, 250, and 300 mm.

2.3. Characterization of Ag-Doped Coating Samples. To obtain information about the size of metal clusters embedded in the coating, grazing-incidence small-angle X-ray scattering (GISAXS) measurements were carried out on a Xenocs Xeuss 2.0 instrument equipped with a Cu Kα source collimated by two sets of scatterless slits. A Pilatus 300k detector mounted on a translation stage was used to record the scattered signal. Measurements were made with a sample to detector distance of 1.188(5) m giving a 1−82 nm particle size range or a sample to detector distance of 0.540(5) m giving a 1−35 nm particle size range. The distance was calibrated using a silver behenate standard. More details on the GISAXS measurements and data analysis can be found in the Supporting Information.

A TESCAN MIRA-3 scanning electron microscope (SEM) equipped with an Oxford Instruments XMax silicon drift detector (SDD) for energy dispersive X-ray spectroscopy (EDS) was used for the microstructural characterization and chemical analysis at 10 kV. Images at a magnification of 50 000 were taken to investigate the aging of the sample surface, and EDS analysis was performed to measure the concentration of Ag and Cu in the coating.

2.4. Antimicrobial Property Measurement. To measure the antimicrobial performance of the carbon coating samples, two approaches have been taken, i.e., antimicrobial tests under terrestrial gravity and under microgravity conditions.

2.4.1. Terrestrial gravity. For the antimicrobial tests under terrestrial gravity conditions, the procedure specified in the ISO standard ISO 22196:2011(E) was followed, with the following modifications. The standard stipulates that test samples are 50 mm × 50 mm, whereas the samples used in the study were 25 mm × 25 mm. Thus, the test area upon the surface was reduced to a 17 mm × 17 mm square, resulting in a 4 mm border around the test area. The number of colony forming units of a culture of *E. coli*, grown overnight in LB broth, was determined, and the concentration adjusted such that a 40 μL aliquot contained 44 000 individual cells. Once applied to the test surface area, this equated to 15 224 cells/cm^2 of test area: comparable to the 15 000 cells/cm^2 as stipulated in the ISO standard. Following inoculation, the procedure stipulated in ISO 22196:2011(E) was followed.

2.4.2. Microgravity. For the antimicrobial tests under microgravity conditions, the same Ag-doped carbon coatings were deposited on smaller stainless steel substrates with dimensions of 10 mm × 10 mm × 3 mm, as required by the microgravity facility. The carbon coating samples were first soaked in ethanol (75%) solution for 1 h in the dark, to remove any contaminations on the surface, then incubated in *E. coli* solution (10^6 cfu mL^{-1}) for 24 h under microgravity conditions. They were then removed from the solution in a laminar flow cabinet and rinsed with a 0.1 M PBS (phosphate-buffered saline) solution to wash off any loosely attached bacteria and then put into a 5 mL Eppendorf tube filled with PBS solution. The Eppendorf tube was then shaken on an orbital shaker, to transfer the bacteria from the coating surface to the solution. The bacteria/PBS solution was diluted multiple times, and the number of bacteria was counted on a plate.

For both antimicrobial tests, a blank stainless-steel 304 substrate coated with carbon only was used as a control sample. The antibacterial efficiency has been quantified from the bacteria killing rate K as follows:

$$K = \frac{N_C - N}{N_C} \times 100\% \tag{1}$$

where N_C is the number of bacteria in the control group while N is the number of bacteria retrieved from the sample being tested.

2.5. Silver Ion Release Experiment. To reveal any possible correlation between antimicrobial activity and Ag$^+$ ion release rate, inductively coupled plasma mass spectrometry (ICP-MS) measurements were carried out. Samples were soaked in 25 mL of nutritional broth for 24 h at 35 °C, following the same protocol as detailed in ISO 22196:2011(E). Ag embedded in a matrix of carbon would eventually release some Ag into the solution in the form of Ag$^+$ ions. It is assumed that the Ag concentration in the solution is proportional to the corresponding sample's Ag leaching rate.

Solution samples were analyzed using a Perkin Emer Elan 6000 ICP-MS. Solutions were initially digested with trace metal grade nitric acid and trace metal grade hydrogen peroxide. They were then diluted (×50) with ultrapure water and an internal standard added ready for ICP-MS analysis. To avoid possible interferences, standards were prepared by adding known amounts of silver to reference stock broth solution samples. These were then prepared for ICP-MS analysis in the same way as the test solution samples.

2.6. Mechanical and Tribological Properties. Wear and friction characteristics were assessed using a TCL Pin-On-Disc test machine and followed the procedure of ASTM G99-17. A 40 N test load was applied to a 5 mm diameter WC/6 wt % Co ball, contacting the coating surface which was rotating at 382 rpm, to produce a linear test speed of 200 mm s^{-1} on a 10 mm diameter wear track. Test were carried out dry and at room temperature and humidity. The friction coefficient was recorded throughout the 1 h test. The test load chosen (40 N) was high in comparison to the ASTM G99-17 requirements (10 N) but designed to produce high contact pressures that similar a-C coatings, without antimicrobial additives, can withstand with good performance. The calculation of the specific wear rate (SWR) of the coatings also followed the procedures specified by the same ASTM standard G99-17.

Coating hardness was measured using a Fischerscope HM2000 microhardness tester to the standard DIN EN ISO 14577-1,2,3, with maximum test load 50 mN. At least 5 indentations (load/unload cycles) were performed on each coating.

To measure coating thickness (following ASTM standard E1182-93), a 30 mm diameter ball was rotated against the coating surface, with diamond paste applied, to produce a tapered section through the coating. An optical system with associated software, was used to view the crater produced, and to select coating layers within. The thicknesses of the layers were calculated by the software based on the ball diameter and geometry.

3. RESULTS AND DISCUSSION

3.1. Mechanical Properties. Amorphous carbon (a-C) coatings have attracted great interest because of their properties such as chemical inertness, superhardness, super low friction, excellent thermal conductivity similar to metals,

Table 1. Hardness and Wear Characteristics of Ag- and Cu-Doped a-C Coating Samples

sample number[a]	composition			wear characteristics			hardness (GPa)
	Ag concentration (atomic, %)	Cu concentration (atomic, %)	thickness (μm)[b]	coefficient of friction[c]	specific wear rate ($\times 10^{-17}$ m^3/Nm)		
A1	6.9 ± 1.2	0.0	1.62	0.09	7.4 ± 1.5		21.8 ± 6.4%
A2	10.8 ± 0.4	0.0	1.68	0.04	4.5 ± 1.2		21.9 ± 8.8%
A3	15.7 ± 2.1	0.0	1.62	0.06	4.9 ± 1.1		22.4 ± 8.8%
A4	17.7 ± 1.7	0.0	1.74	0.09	2.8 ± 0.9		21.3 ± 7.9%
B1	8.2 ± 0.3	6.0 ± 0.2	1.75	0.16	6.0 ± 1.0		21.9 ± 9.3%
B2	13.4 ± 0.2	5.7 ± 0.1	1.92	0.13	7.4 ± 0.9		19.5 ± 6.9%
B3	16.1 ± 0.1	6.2 ± 0.3	1.94	0.11	7.5 ± 0.9		18.6 ± 10.3%
B4	17.1 ± 0.2	5.6 ± 0.2	1.97	0.12	11.3 ± 1.1		19.6 ± 2.9%
C1	1.5 ± 0.1	14.5 ± 0.6	1.50	0.15	16.8 ± 1.5		32.2 ± 22.6%
C2	4.5 ± 0.2	7.1 ± 0.2	1.40	0.17	4.6 ± 1.0		29.2 ± 18.7%
C3	6.6 ± 0.5	1.8 ± 0.1	1.40	0.15	7.7 ± 1.2		27.9 ± 9.2%
NP1	2.37 ± 0.32	0.0	1.02	0.10	9.9 ± 1.2		17.4 ± 4.2%
NP2	1.55 ± 0.59	0.0	0.90	0.09	3.8 ± 0.9		16.3 ± 8.7%
NP3	3.54 ± 0.61	0.0	1.00	0.12	5.5 ± 1.1		14.3 ± 3.3%

[a]Samples from A1 to C3 were prepared by cosputtering of Ag, Cu, and carbon in the same vacuum chamber, following the procedure described in section 2.1. The remaining three samples from NP1 to NP3 were Ag-cluster-doped a-C coatings, utilizing the cluster source and following the preparation procedure described in section 2.2. [b]Total coating thickness including a chromium adhesion layer of 0.27 μm. All measurements have an error of ±0.1 μm. [c]The measurement error for the coefficient of friction is less than 10% for all samples.

extremely smooth surface, wear resistance, and corrosion resistance.[55] These films have particular advantages in demanding environments and have found wide application in the automotive industry (diesel injection systems, tappets, piston pins, and others),[56] motorsport industry,[57] micro-electromechanical systems, bearings, machine tools and dies,[55] and even in the harsh conditions of low Earth orbit (on the exterior of the International Space Station).[58]

Depending on the preparation method and application requirement, the amorphous carbon coatings can be hydrogenated, normally written as a-C:H. The a-C coatings in this work were non-hydrogenated and deposited using unbalanced magnetrons in a closed field arrangement (shown on the right-hand side of Figure 1). Excellent coating adhesion was achieved by using a chromium interlayer. The coating structure for earlier coatings has been found to be dense and amorphous, although high resolution TEM detected fine regions of nanocrystalline graphite within the amorphous carbon matrix.[59] Raman analysis of earlier coatings indicated that the coating is mostly sp^2 bonded carbon.[59]

The hardness of a-C coatings, dependent on the deposition parameters, is typically 15−25 GPa but can be over 40 GPa. The coefficient of friction is dependent on the load and counter-face material but is generally below 0.1. The introduction of Ag and Cu into the carbon matrix will inevitably make an impact on such coatings' mechanical properties. The hardness and friction coefficient of various Ag- and Cu-doped a-C coatings were measured and summarized in Table 1.

Among all the samples, the Ag dopant concentration ranged from 1.5% to ∼18% (atomic), while the Cu concentration was up to 14.5% for Cu-doped samples. Samples A1 to A4, and NP1 to NP3, contained Ag only, and their coefficient of friction is still below 0.1. For samples with Cu added, the friction coefficient is higher, in the range 0.11 to ∼0.17, which is still considered to be a reasonably low friction. The hardness is measured at ∼14 GPa or higher, and the specific wear rate is ∼1.0 × 10^{-16} m^3/Nm, all of which have indicated that the key metrics of the mechanical properties have been maintained

despite the doping of Ag/Cu at various level. As a result, it is expected that these Ag/Cu-doped a-C coatings should perform reasonably well in a wide range of applications in a very demanding environment.

3.2. Metal Particle Size. During the coating deposition process, the substrate was continuously rotating at a speed of 5 rpm on a cylindrical drum, taking approximately 1 s to pass each sputtering target for each rotation. When the substrate is facing the Ag target, a large number of sputtered Ag atoms arrive at the substrate surface together with small amount of stray carbon atoms. Most of the sputtered atoms have a kinetic energy of ∼2 eV but can go up to 10−20 eV, even 100 eV.[60,61] When these energetic atoms land at the surface, they immediately become mobile and diffuse laterally on the surface until they are trapped by a surface defect or collide with another Ag atom or particle and bind together. The silver atom and carbon atom do not bind together chemically to form a compound; therefore, Ag exists in the form of either single atoms or particles in the matrix of the amorphous carbon structure.

The probability of colliding and binding increases with the number of Ag atoms deposited, i.e. the deposition rate of Ag, which also affects the final Ag concentration in the coating. Studies conducted by other research groups have shown that both higher Ag concentration[62,63] and higher substrate temperature during deposition[33,34] can lead to the formation of bigger size Ag particles. The results in this work as shown below are in line with those findings.

It has been reported that the size of Ag nanoparticles has a strong influence on their antimicrobial performance.[29−31] Therefore, it would be highly interesting, from both scientific and application perspective, to determine the size of Ag particles produced in this work and, then, investigate whether the antimicrobial performance is indeed dependent on the particle size. However, it was found to be very challenging to experimentally measure the particle size distribution in a nanocomposite coating. The standard transmission electron microscopy (TEM) approach was considered but presented two shortcomings: (i) it is very difficult to prepare a thin slice

of coating as a TEM specimen without causing oxidation to the Ag particles and (ii) even if the TEM sample preparation was successful, TEM can only observe a tiny section of the sample, and it was debatable whether this tiny section could represent the overall particle size distribution of the whole sample. Instead of TEM, it was decided to use the relatively new technique, grazing incidence small angle X-ray scattering (GISAXS), as a nondestructive analytical approach to determine the Ag particle size distribution in the a-C coatings.

Figure 2 shows the particle size distribution results given by GISAXS measurement for three selected samples: A1 (6.9%
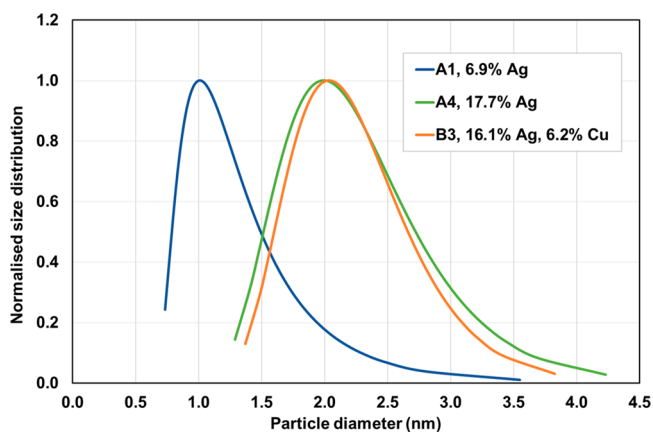

Figure 2. Size distribution of Ag particles embedded in a-C coatings measured by GISAXS: sample A1 (6.9% Ag, blue), sample A4 (17.7% Ag, dark green), and sample B3 (16.1% Ag and 6.2% Cu, orange).

Ag), A4 (17.7% Ag), and B3 (16.1% Ag and 6.2% Cu). It can be seen that for low Ag content sample A1, the particle size peaks at 1 nm in diameter, but it can go up to 2.5 nm albeit with very small amount. The overall size distribution is quite narrow, with a log-normal shape. It is not so surprising to see the narrow size distribution, as there is very limited time available for deposited Ag atoms to diffuse, collide, and grow into bigger particles in each rotation of the cylindrical drum. When the sputtering rate of Ag was increased by turning up the sputtering power on the Ag target, the metal particle size grew bigger to about 2 nm for samples A4 and B3 (Figure 2). The

size distribution also becomes slightly broadened, compared with sample A1. More detailed information on the analysis of the GISAXS spectra and the extrapolation of the size distributions shown in Figure 2 can be found in the Supporting Information.

During the GISAXS analysis, the X-ray scattering from a sample was monitored and measured by a detector, and the difference in the wavenumber between the scattered and incident light calculated. For a particle inside a medium, the bigger the particle, the larger the difference in the electron density between the particle and the medium and, hence, the better it scatters X-rays. For this reason, particles with diameters less than 1 nm are very difficult to detect with this technique, since they have a much lower scattering efficiency. The result is that those small particles, including Ag single atoms, are not truly reflected in the GISAXS spectra analysis. For example, in Figure 2 the size distribution plot for sample A1 seems to indicate that there are no single Ag atoms at all in the carbon matrix, which is highly unlikely. On the contrary, it is expected that there should be a considerable amount of single Ag atoms existing inside the a-C coating, as the deposition rate of carbon is more than 10 times faster than that of silver and there should be a quantity of Ag atoms embedded in the matrix before they diffuse far enough to collide with other Ag species.

Both samples A4 and B3 have similar amounts of Ag content in the coating and show very similar size distribution profiles for metal particles. Interestingly, the normalized intensity drops to a value below 0.2 at a particle size of 1.2−1.3 nm, which is higher than the lower detection limit of GISAXS. This seems to suggest that the concentration of single Ag atoms is indeed very low in these two samples. It is speculated that for higher metal concentration samples, chances of having metal single atoms dispersed in the coating are slimmer as the deposited metal atoms preferentially grow into bigger particles. Sample B3 also contains 6.2% of Cu, but GISAXS could not distinguish the two doping elements, so no valuable information could be extracted on the possible structure and composition of Ag/Cu particles.

Generally speaking, the size of metal particle dopants embedded in a coating matrix could be influenced by many factors, including the deposition rate of dopant (Ag or Cu in
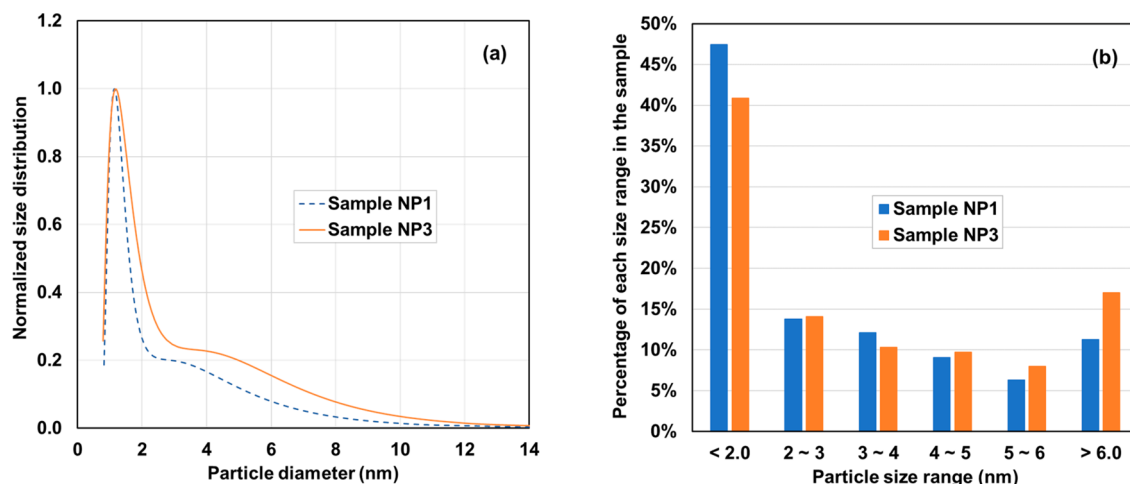

Figure 3. (a) Size distributions from GISAXS spectra for Ag-cluster samples prepared at two different aggregation lengths: 200 mm (sample NP1) and 300 mm (sample NP3). (b) Histogram of these two samples in six particle size ranges.

this case), the deposition rate of the matrix (carbon in this case), the intermixing nature of the dopant and matrix, the mobility of dopant on the surface, the substrate temperature, the rotation speed of the cylindrical drum, the sputtering gas pressure, the bias voltage applied on the substrate, and so on. In the majority of cases, these factors are interlinked and cannot be independently changed without affecting something else. For instance, it has been shown that the Ag particle size can grow bigger by increasing the Ag deposition rate. However, this also leads to a higher Ag concentration in the carbon matrix. It is almost impossible to produce a sample with bigger Ag particles while at the same time keeping a uniform low percentage in the a-C coating, via the cosputtering approach. This limitation has severely restricted one's capability of finely tuning the Ag-doped nanocomposite coating properties, including hardness, friction coefficient, electrical conductivity, and antimicrobial property, etc., to their optimum state.

The approach taken in an attempt to address this challenge was to separate the Ag particle growth process from the carbon deposition process. A cluster source was used to produce Ag particles in a separate chamber, while the main deposition chamber was used for carbon deposition only. The Ag particle size can be tuned in the cluster source chamber by varying the aggregation length and Ar gas flow rate, while the percentage of Ag content in the a-C coating can be controlled by adjusting the deposition rate of carbon in the main chamber. In this way, the link between Ag particle size and Ag concentration has been broken, thus providing a flexible technical route to produce versatile nanocomposite materials.

Three Ag-cluster-doped a-C coating samples have been prepared with aggregation lengths of 200 mm (sample *NP1*), 250 mm (*NP2*), and 300 mm (*NP3*), respectively. Samples *NP1* and *NP3* were selected for GISAXS analysis, and the result is shown in Figure 3. Both samples have shown a bimodal size distribution, which seems to be unusual as a single peak might be expected. However, this is not something uncommon for such cluster sources, as Haberland also reported that distributions with two or three maxima had been observed.[64] It is believed that by finely tuning the cluster source parameters, for example the sputtering power and Ar flow rate, one should be able to achieve a size distribution with one single peak.

Nevertheless, the majority of the Ag clusters (40−50%, Figure 3b) embedded in both a-C coating samples have a similar size, with diameters of around 1.2 nm, as seen in the first peaks in Figure 3a. For the second peaks (or shoulders) in Figure 3a, the Ag clusters in sample *NP1* have a peak position ∼3.2 nm, while the Ag clusters in *NP3* are bigger at ∼4.2 nm. The bigger size in sample *NP3* is expected as it follows the general trend that the cluster size increases with the aggregation length. With the increase of aggregation length, the clusters have longer residence time inside the condensation chamber, and Ag particles have more time available to collide with other Ag single atoms (or other Ag particles) thus growing larger. Cluster size distributions from GISAXS are in agreement with our previous results[41] as well as with studies from other research groups.[38,39]

Table 2 compares the particle size distributions for the samples prepared by cosputtering, (samples *A1*, *A4*, and *B3*), and the samples prepared by the combined cluster-source deposition technique (samples *NP1* and *NP3*). Although the Ag concentrations in *NP1* and *NP3* are much lower at 2.4% or 3.5%, they have a much broader size distribution and contain a

Table 2. Comparison of Particle Size Distribution between Different Samples Based on GISAXS Results[a]

Sample number	Ag %	Particle size range (nm)					
		< 2.0	2 - 3	3 - 4	4 - 5	5 - 6	> 6.0
A1	6.9%	0.74	0.08	0.08	0.00	0.00	0.00
A4	17.7%	0.47	0.68	0.15	0.01	0.00	0.00
B3	16.1%	0.39	0.66	0.09	0.00	0.00	0.00
NP1	2.4%	0.73	0.21	0.19	0.14	0.10	0.17
NP3	3.5%	0.90	0.31	0.23	0.21	0.18	0.38

[a]The numbers in the table are the areas under a curve calculated for each plot in Figures 2 and 3a, which represent the relative quantity of clusters in each particle size range. The darker the color, the greater the number of clusters in that particle size range.

lot more of the bigger Ag particles. This demonstrates the advantage of using a cluster source to control both the Ag concentration and Ag particle size at the same time.

Another point that should be stressed, is that, due to the high pressure within the condensation chamber, single atoms which do not merge into clusters have low probability of being dragged out from the chamber by the carrier gas along with clusters, since they have higher Brownian diffusivity and therefore a higher chance to be deposited on the walls of the condensation chamber.[41] As a result, the cluster-beam produced in the main deposition chamber contains only Ag particles along with a small portion of carrier gas, and hence very few or no single Ag atoms should be found in the samples of *NP1−NP3*.

3.3. Aging Test. To understand how samples degrade over time, SEM images of the sample surface have been taken after 16, 30, and 59 weeks of deposition. Samples with different Ag concentrations and their surface evolution are shown in Figure 4.

For Ag concentrations lower than 10.75%, metal whiskers on the surface increase with the Ag content. For higher Ag
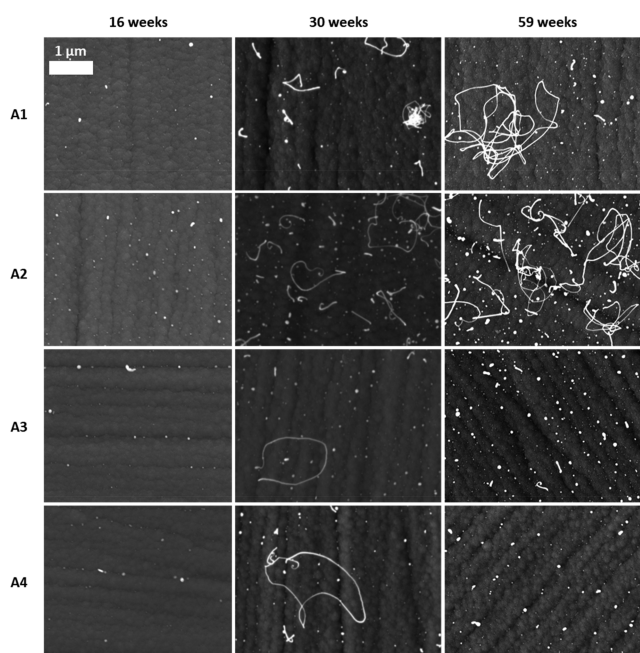

Figure 4. SEM images showing the aging of the Ag-doped amorphous carbon coating for different Ag concentrations. Images were taken at 16, 30, and 59 weeks after sample preparation.

concentration, metal whisker formation starts to be inhibited. As mentioned in section 3.2, for samples prepared with a higher Ag content, Ag atoms preferably form big particles and the amount of Ag single atoms in the a-C coating is limited. It is believed that bigger particles have lower mobility compared to smaller ones, and single atoms have the highest mobility. Metal atoms would randomly diffuse inside the coating through the gaps and tunnels between the sp[2] hybrid bonded carbon microstructure and eventually reach the surface, where their mobility is higher than in the bulk. It is very likely that the moisture in the air plays a critical role in the formation of the whiskers as shown in SEM images.[24,28] With an increase in Ag concentration, the amount of Ag single atoms increases, and whisker production is amplified. If Ag content is further increased, however, more Ag atoms starts forming bigger particles which have lower mobility, and the concentration of Ag single atoms dispersed in the coating decreases, therefore hindering the whisker production.

If Cu is added along with Ag during the deposition process, samples do not show whiskers on the surface even after 61 weeks. Figure 5 shows SEM images for Ag−Cu-doped a-C
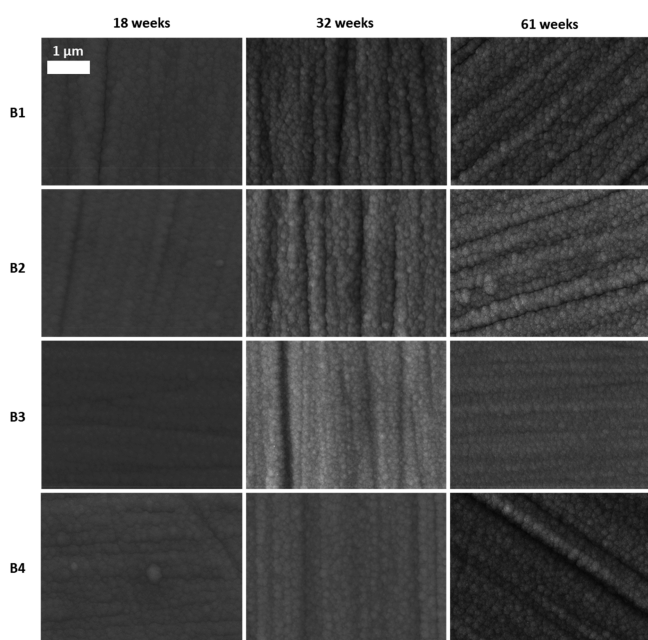

Figure 5. SEM images showing the aging of the Ag−Cu-doped amorphous carbon coating for different Ag concentrations. Images were taken at 18, 32, and 61 weeks after sample preparation.

coatings, taken at 18, 32, and 61 weeks after sample preparation. It is remarkable to see how the surface is preserved and no metal particle or whisker can be detected, even after more than one year after sample preparation. One possible reason could be that Cu would obstruct the gaps in the carbon matrix, limiting Ag diffusion to the surface of the samples.[65,66] According to refs 65 and 66, incorporating Cu in the amorphous carbon matrix would have beneficial effects on the coating, i.e. reducing its stress, filling interstitial gaps, and in sufficient concentration, forming nanoclusters and then nanocrystallites in the carbon matrix. The combination of these effects can potentially reduce the Ag migration, increasing the coating durability.

For samples NP1, NP2, and NP3 prepared with a combination of cluster-source and conventional magnetrons,

they do not have single Ag atoms embedded in the carbon matrix, and all the Ag inside the coating is in the form of particles, i.e. with mobility much lower than single atoms. SEM images for Ag-cluster samples (Figure 6) show that the sample
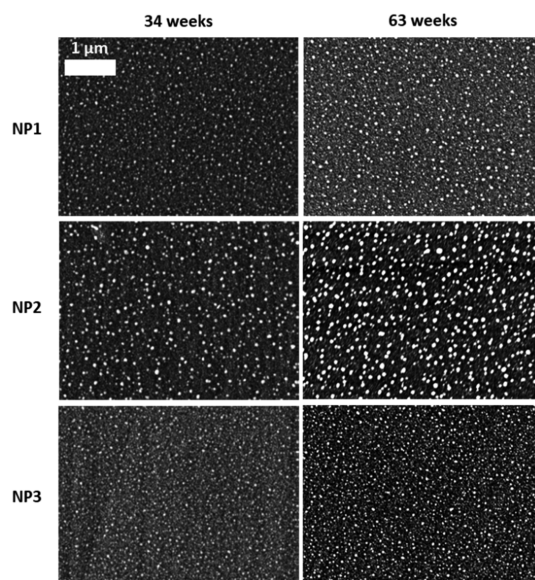

Figure 6. SEM images showing the aging of the Ag-cluster-doped amorphous carbon coating for different aggregation lengths. Images were taken at 34 and 63 weeks after sample preparation.

surface is not affected by whisker formation, and even after 63 weeks, no Ag whiskers were observable on the sample surface. The majority of the densely populated white dots on the surface are not considered to be individual Ag clusters generated by the cluster source, because the sizes of the dots in the SEM images can be up to 30 or 40 nm in diameter, which is beyond the upper limit of cluster size that a cluster source can produce. More likely, these white dots are the results of the agglomeration of many Ag clusters on the surface. Because during the deposition process, the carbon sputtering was switched off several seconds earlier than the cluster source, the sample surface was covered with a thin layer of Ag clusters. These Ag clusters on the surface can diffuse and agglomerate into bigger particles.

Similarly to Ag−Cu-doped a-C coatings, Ag-cluster-doped a-C samples also show a very stable surface morphology but with a much lower Ag concentration.

3.4. Ag⁺ Ion Release. The size-dependent antibacterial efficacy of silver nanoparticles (AgNPs) synthesized by the wet chemistry approach (coreduction) has been reported by Agnihotri et al.[29] For AgNPs stabilized by citrate with a size from 5 to 100 nm, it was found that, when the sizes are less than 10 nm, the antibacterial efficacy is significantly enhanced, and 5 nm demonstrates the best results and mediates the fastest bactericidal activity. However, Alvarez et al. argued that the particle size effect is negligible on the antibacterial activity of AgNPs.[31] They demonstrated, instead, that the toxicity of various AgNPs (PEG- or PVP-coated, of three different sizes each) accurately follows the dose−response pattern of *E. coli* exposed to Ag⁺ ions. This suggested that AgNP morphological properties (particle size, etc.) primarily influence Ag⁺ ion release, which then affect antimicrobial activity in an indirect way.[31]
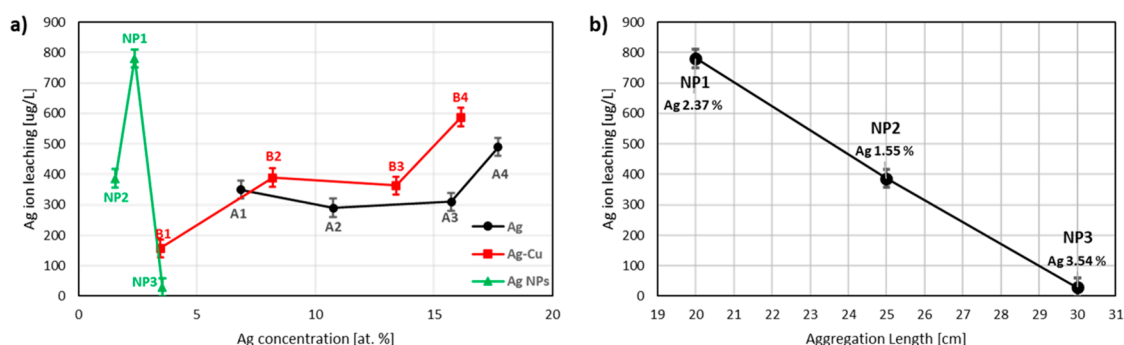
Figure 7. Ag⁺ ion concentration measured by ICP-MS after immersion of samples in nutritional broth solutions, as detailed in ISO 22196:2011(E), for 24 h. (a) Ag⁺ ion concentration in the nutritional broth after sample immersion for 24 h at 35 °C as a function of the Ag concentration in the coating for Ag (black circles), Ag−Cu (red squares), and Ag-cluster-doped samples (green triangles). (b) Ag⁺ ion concentration in the nutritional broth after sample immersion for 24 h at 35 °C as a function of the aggregation length for Ag-cluster samples.
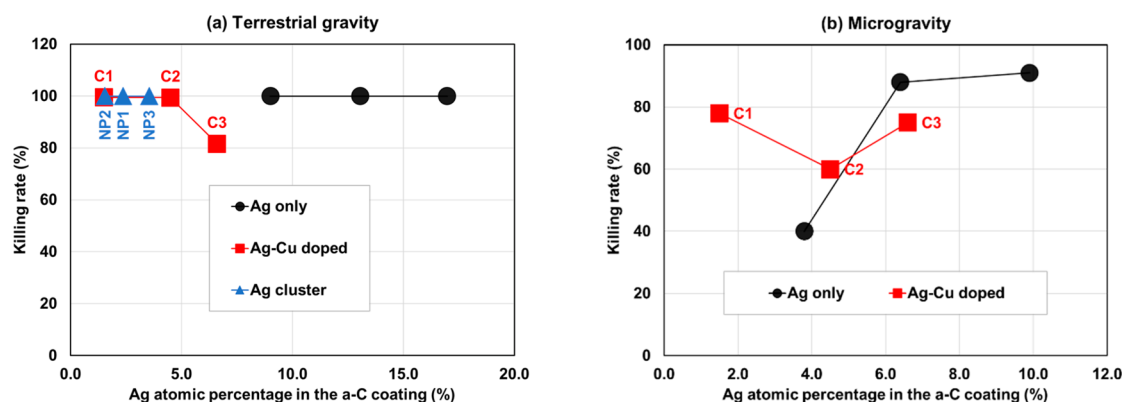

Figure 8. Antimicrobial activity of selected amorphous carbon coating samples as a function of Ag concentration against *E. coli*. (a) Killing rate of Ag-doped (black circles), Ag−Cu-doped (red squares), and Ag-cluster-doped (blue triangle) a-C coatings, under terrestrial gravity conditions (in a normal lab), following the ISO 22196:2011(E) protocol. (b) Killing rate of Ag-doped (black circles) and Ag−Cu-doped (red squares) a-C coatings, under microgravity conditions (in a lab with a ground-based microgravity facility), following the protocol described in section 2.4.2.

For Ag-doped coatings prepared by a physical approach (magnetron sputtering), it has been shown that the Ag⁺ ion release rate increases with the increase of Ag concentration inside a TiO₂ thin film.[67] Samples prepared in this work (via cosputtering or cluster source approach) were investigated for a similar pattern concerning Ag release or evidence of different behavior.

Ag⁺ ion release experiments (Figure 7), running under similar conditions to the ISO-22196 standard antimicrobial test, confirmed that a higher Ag concentration increased the amount of Ag⁺ ions released into the solution from the samples prepared by the cosputtering approach. The presence of Cu in the coating did not seem to influence this trend (Figure 7a).

However, for the samples prepared by the cluster source approach, the Ag⁺ ion release did not show an obvious correlation with the Ag concentration in the a-C coating, as shown in Figure 7a. Instead, the Ag⁺ ion release rate reduced linearly with the increase in aggregation length, which related to an increase in Ag-cluster size from samples NP1−NP3 (Figure 7b). Chen et al. developed a kinetic model to describe the Ag⁺ release for citrate-coated AgNPs based on the hard sphere theory using the Arrhenius equation.[30] For the 20, 40, and 80 nm AgNPs they studied, Ag⁺ release rates were found to depend on primary particle size and concentration in solution. In this work, although the Ag clusters in the a-C coating have a much smaller size, with majority of them being smaller than 6 nm, they seem still to follow the same ion

release kinetics where a smaller particle size is beneficial for a higher Ag⁺ ion release rate.

Comparing the three curves in Figure 7a carefully, it is striking that the sample NP1, with a silver concentration of only 2.37% prepared by the shortest aggregation length via the cluster source approach, has a higher Ag⁺ ion release rate than that of sample A4, which contains 7 times more Ag in the a-C matrix at 17.7%. For sample NP2, the Ag concentration is even lower at 1.55%, but its Ag⁺ ion release is on par with all those A series and B series samples, which have much higher Ag percentages. The ion release is significantly reduced when the Ag-cluster size grows bigger in sample NP3 at an aggregation length of 300 mm.

It has been shown that the smaller the Ag particle, the higher the ion release rate; and the higher the Ag concentration in the coating, the higher the ion release rate. However, it is not well understood why sample NP1 with a low concentration has the highest Ag⁺ ion release rate among all a-C coating samples. Further systematic investigations are needed to reveal the elusive mechanism.

Nevertheless, as a higher Ag⁺ ion release rate is correlated to a higher antimicrobial efficacy,[31] the samples prepared by the cluster source approach look more promising for antimicrobial applications, as they combine a high Ag⁺ ion release rate with a more stable surface morphology (Figure 6).

3.5. Antimicrobial Test. To evaluate the antimicrobial efficacy of the Ag-doped a-C coatings, antimicrobial tests were

carried out on selected samples, either in a normal lab under terrestrial gravity or in a ground-based lab with microgravity facility, simulating the condition in a space station.

In the case of the terrestrial gravity tests, the international standard ISO 22196:2011(E) was followed to measure antibacterial activity, which allowed benchmarking the performance of coatings against similar antimicrobial products. Briefly, coated samples were inoculated with a known amount of bacteria, before being incubated for 24 h. After this time, the bacteria were recovered, and the number of viable bacteria determined for each coated sample. The results, shown in Figure 8a, are presented as the percentage killing rate of Ag-doped, Ag−Cu-doped, and Ag-cluster-doped coatings compared to an amorphous carbon coating containing no antimicrobial metals. The results show that both Ag- and Ag-cluster-doped samples killed completely all of the inoculated bacteria, since no bacteria were recovered after 24 h incubation, compared to a metal free coating. The Ag−Cu-doped coatings were not as effective; however, during the 24-h time period, the worst performing coating still killed 81.6% of the bacteria.

It should be noted here that an Ag concentration as low as 1.5% was found to be sufficient to be highly effective as a bactericide, which could have a couple of important implications. First, a low Ag content will minimize the influence of metal dopants on the mechanical properties of the coating. This is a sought-after advantage, as a successful antimicrobial engineering coating should be characterized by an excellent antimicrobial activity with desired mechanical strength and wear resistance. Second, the low Ag content also means that there would be much less heavy metal (Ag in this case) potentially leaching to the environment and causing health concerns during the lifetime of products with these coatings.

It should be considered that any future development of Ag-containing antimicrobial coatings could limit the Ag concentration to a level below 5%, to minimize the leaching level.

For samples doped with Ag only, tests done under microgravity conditions (Figure 8b) show that a higher content of Ag is in general beneficial to the bactericidal properties, which is in agreement with similar experiments done under terrestrial gravity conditions.[31,68] When both Ag and Cu are doped into the a-C coatings, a clear trend is not observed, but a killing rate above 60% is maintained for all three samples. Because of the very limited access to the microgravity facility, the Ag-cluster-doped samples were not managed to be tested. However, based on the Ag$^+$ ion release result and the antimicrobial test result in terrestrial gravity conditions, it is estimated that the Ag-cluster-doped samples should perform well under microgravity conditions.

Because of the restrictions on the sample size and the facilities available from the microgravity lab, a different protocol (other than the international standard) has been followed to measure the antimicrobial activity under microgravity conditions, which makes it impossible to directly compare the results in Figure 8a and b. However, it is apparent that a high Ag content is beneficial for antimicrobial activity, and the addition of Cu does not significantly influence the coatings' antimicrobial activity.

It has been demonstrated that microgravity, whether found in a space station or in a ground-based facility, and the low fluid shear dynamics associated with microgravity play a key role in the regulation of microbial gene expression, physiology,

and pathogenesis.[69] Many studies showed that microorganisms grew more densely, with a growth curve characterized by a decreased lag phase and a prolonged exponential phase.[69] A recent study carried out on the International Space Station (ISS) confirmed that microorganisms grow better in space than on Earth. For example, *E. coli* cultured on board the ISS showed a 13-fold increase in the final cell count compared with the ground control after 49 h.[70] The lower antimicrobial activity observed in Figure 8b might be related to the faster multiplication of *E. coli* under microgravity conditions.

However, another factor that cannot be ruled out is the different antimicrobial testing protocols adopted for the terrestrial gravity experiments and the microgravity experiments. For the ISO standard method used for the terrestrial gravity tests, only the sample surface covered with the coating was exposed to the bacteria culture solution, while, in the case of the microgravity protocol, the whole sample was immersed in the bacteria solution. For all the stainless-steel plates used as substrates, only top side of the plate was coated with the carbon coating, while the back side was left bare. When the whole sample was immersed in the bacteria solution, the noncoated back side of the sample played no role in inhibiting the growth of *E. coli*. It is suspected that this difference might have contributed to the lower killing rate in the case of microgravity. To truly reveal the influence of microgravity on the antimicrobial properties of the coatings, future development work should include the design of a new testing protocol suitable for both terrestrial gravity and microgravity experiments.

4. CONCLUSIONS

It has been demonstrated that all the antimicrobial amorphous carbon coatings developed in this work have maintained their excellent mechanical properties, including high hardness, low friction coefficient, and good adhesion, despite the fact that the doped metal content was as high as 17.7% (atomic) in some cases. This creates a solid foundation for further development of long lifetime antimicrobial surfaces for application in manned spacecraft.

The durability of the antimicrobial surfaces is the major challenge that needs to be addressed. In this work, the stability of coating surface morphology has been investigated up to 63 weeks after deposition. It has been shown that the Ag-doped a-C coating samples prepared by cosputtering presented extensive growth of metal whiskers after 30 weeks, which can be explained by the high mobility of single silver atoms embedded in the amorphous carbon matrix. By the addition of copper via cosputtering or taking the cluster-source approach, the whisker structures were no longer visible after more than 60 weeks. This seems to suggest a much-improved durability.

Both the durability and the Ag$^+$ ion release rate can be correlated to the metal particle size distribution in the coating matrix. The cluster-source approach has demonstrated a great advantage in its capability to tune the particle size and the metal concentration independently. It is expected that, in addition to antimicrobial coatings, this flexible and versatile technical route would be able to make many novel nano-composite materials with interesting microstructures for applications in other areas.

The antimicrobial tests, carried out under both terrestrial gravity and microgravity conditions, showed extremely high levels of antimicrobial activity for nearly all the samples. Even

an Ag concentration as low as 1.5% was found to be highly effective.

To select a good candidate for onboard antimicrobial testing in a space station, it may be preferable to rule out Ag-only-doped a-C coatings prepared by cosputtering, without considerable further development work, because of the formation of whiskers in a relatively short period, implying an undesirable higher level of metal leaching to the environment. New approaches such as multilayering may be necessary to reduce these problems. In contrast, either Ag−Cu or Ag-cluster-doped a-C coatings could be suitable candidates immediately, with a suggested silver concentration lower than 5%. Further investigations are needed to better understand the silver diffusion within the matrix and how this would influence the antimicrobial property in a much longer time frame.

■ ASSOCIATED CONTENT

ⓈI Supporting Information

The Supporting Information is available free of charge at https://pubs.acs.org/doi/10.1021/acsami.2c00263.

Details about GISAXS measurement and data analysis (PDF)

■ AUTHOR INFORMATION

Corresponding Author

Jinlong Yin − *Teer Coatings Ltd., Droitwich, Worcestershire WR9 9AS, United Kingdom;* ⓞ orcid.org/0000-0002-8770-3141; Email: jinlong.yin@teercoatings.co.uk

Authors

Giuseppe Sanzone − *Teer Coatings Ltd., Droitwich, Worcestershire WR9 9AS, United Kingdom; Quantum Solid-State Physics, Department of Physics and Astronomy, KU Leuven, B-3001 Leuven, Belgium*

Susan Field − *Teer Coatings Ltd., Droitwich, Worcestershire WR9 9AS, United Kingdom*

David Lee − *Department of Life Sciences, School of Health Sciences, Birmingham City University, Birmingham B15 3TN, United Kingdom*

Jingzhou Liu − *Shanghai Aerospace Equipment Manufacturer, Minhang, Shanghai 200245, China*

Pengfei Ju − *Shanghai Aerospace Equipment Manufacturer, Minhang, Shanghai 200245, China*

Minshi Wang − *School of Metallurgy and Materials, University of Birmingham, Birmingham B15 2TT, United Kingdom*

Parnia Navabpour − *Teer Coatings Ltd., Droitwich, Worcestershire WR9 9AS, United Kingdom*

Hailin Sun − *Teer Coatings Ltd., Droitwich, Worcestershire WR9 9AS, United Kingdom*

Peter Lievens − *Quantum Solid-State Physics, Department of Physics and Astronomy, KU Leuven, B-3001 Leuven, Belgium*

Complete contact information is available at:
https://pubs.acs.org/10.1021/acsami.2c00263

Notes

The authors declare no competing financial interest.

■ ACKNOWLEDGMENTS

■ REFERENCES

(1) Kim, W.; Tengra, F. K.; Young, Z.; Shong, J.; Marchand, N.; Chan, H. K.; Pangule, R. C.; Parra, M.; Dordick, J. S.; Plawsky, J. L.; Collins, C. H. Spaceflight promotes biofilm formation by Pseudomonas aeruginosa. *PLoS One* **2013**, *8* (4), No. e62437.

(2) Novikova, N. D. Review of the Knowledge of Microbial Contamination of the Russian Manned Spacecraft. *Microbial Ecology* **2004**, *47* (2), 127−132.

(3) Li, L.; Fu, Y.; Liu, H. Development of effective and safe compound disinfectant for space cabins. *Acta Astronautica* **2019**, *159*, 480−485.

(4) Wang, M.; Duday, D.; Scolan, E.; Perbal, S.; Prato, M.; Lasseur, C.; Hołyńska, M. Antimicrobial Surfaces for Applications on Confined Inhabited Space Stations. *Advanced Materials Interfaces* **2021**, *8* (13), 2100118.

(5) Yang, Y.; Wu, X.; He, C.; Huang, J.; Yin, S.; Zhou, M.; Ma, L.; Zhao, W.; Qiu, L.; Cheng, C.; Zhao, C. Metal−Organic Framework/Ag-Based Hybrid Nanoagents for Rapid and Synergistic Bacterial Eradication. *ACS Appl. Mater. Interfaces* **2020**, *12* (12), 13698−13708.

(6) Kelly, P. J.; Li, H.; Whitehead, K. A.; Verran, J.; Arnell, R. D.; Iordanova, I. A study of the antimicrobial and tribological properties of TiN/Ag nanocomposite coatings. *Surf. Coat. Technol.* **2009**, *204* (6), 1137−1140.

(7) Fielding, E. A.; Avelar-Batista Wilson, J. C.; Housden, J. Coated Articles. Patent WO 2009/095705 A2, August 6, 2009.

(8) Lemire, J. A.; Harrison, J. J.; Turner, R. J. Antimicrobial activity of metals: mechanisms, molecular targets and applications. *Nature Reviews Microbiology* **2013**, *11* (6), 371−384.

(9) Han, C.; Lalley, J.; Namboodiri, D.; Cromer, K.; Nadagouda, M. N. Titanium dioxide-based antibacterial surfaces for water treatment. *Current Opinion in Chemical Engineering* **2016**, *11*, 46−51.

(10) Osés, J.; Fuentes, G. G.; Palacio, J. F.; Esparza, J.; García, J. A.; Rodríguez, R. Antibacterial Functionalization of PVD Coatings on Ceramics. *Coatings* **2018**, *8* (5), 197.

(11) Kelly, P. J.; Whitehead, K. A.; Li, H.; Verran, J.; Arnell, R. D. The Influence of Silver Content on the Tribological and Antimicrobial Properties of ZrN/Ag Nanocomposite Coatings. *J. Nanosci. Nanotechnol.* **2011**, *11* (6), 5383−5387.

(12) Lan, W.-C.; Ou, S.-F.; Lin, M.-H.; Ou, K.-L.; Tsai, M.-Y. Development of silver-containing diamond-like carbon for biomedical applications. Part I: Microstructure characteristics, mechanical properties and antibacterial mechanisms. *Ceram. Int.* **2013**, *39* (4), 4099−4104.

(13) Arshad, M.; Qayyum, A.; Shar, G. A.; Soomro, G. A.; Nazir, A.; Munir, B.; Iqbal, M. Zn-doped SiO2 nanoparticles preparation and characterization under the effect of various solvents: Antibacterial, antifungal and photocatlytic performance evaluation. *Journal of Photochemistry and Photobiology B: Biology* **2018**, *185*, 176−183.

(14) Gudkov, S. V.; Burmistrov, D. E.; Serov, D. A.; Rebezov, M. B.; Semenova, A. A.; Lisitsyn, A. B. A Mini Review of Antibacterial Properties of ZnO Nanoparticles. *Frontiers in Physics* **2021**, *9*, 9.

(15) Bonilla-Gameros, L.; Chevallier, P.; Sarkissian, A.; Mantovani, D. Silver-based antibacterial strategies for healthcare-associated infections: Processes, challenges, and regulations. An integrated review. *Nanomedicine: Nanotechnology, Biology and Medicine* **2020**, *24*, 102142.

(16) Edis, Z.; Haj Bloukh, S.; Ashames, A.; Ibrahim, M. Copper-Based Nanoparticles, Their Chemistry and Antibacterial Properties: A Review. *Chemistry for a Clean and Healthy Planet*; Springer: Cham, 2019; pp 401−428.

(17) Gu, X.; Xu, Z.; Gu, L.; Xu, H.; Han, F.; Chen, B.; Pan, X. Preparation and antibacterial properties of gold nanoparticles: a review. *Environmental Chemistry Letters* **2021**, *19* (1), 167−187.

(18) Phan, T. T.; Huynh, T.-C.; Manivasagan, P.; Mondal, S.; Oh, J. An Up-To-Date Review on Biomedical Applications of Palladium Nanoparticles. *Nanomaterials* **2020**, *10* (1), 66.

(19) Safdar, M.; Ozaslan, M.; Khailany, R. A.; Latif, S.; Junejo, Y.; Saeed, M.; Al-Attar, M. S.; Kanabe, B. O. Synthesis, Characterization and Applications of a Novel Platinum-Based Nanoparticles: Catalytic, Antibacterial and Cytotoxic Studies. *Journal of Inorganic and Organometallic Polymers and Materials* **2020**, *30* (7), 2430−2439.

(20) Almoudi, M. M.; Hussein, A. S.; Abu Hassan, M. I.; Mohamad Zain, N. A systematic review on antibacterial activity of zinc against Streptococcus mutans. *Saudi Dental Journal* **2018**, *30* (4), 283−291.

(21) Cochis, A.; Azzimonti, B.; Chiesa, R.; Rimondini, L.; Gasik, M. Metallurgical Gallium Additions to Titanium Alloys Demonstrate a Strong Time-Increasing Antibacterial Activity without any Cellular Toxicity. *ACS Biomaterials Science & Engineering* **2019**, *5* (6), 2815−2820.

(22) Zhang, P.; Zhang, Y.; Sun, Z. Spontaneous Growth of Metal Whiskers on Surfaces of Solids: A Review. *Journal of Materials Science & Technology* **2015**, *31* (7), 675−698.

(23) Schamel, M.; Schopf, C.; Linsler, D.; Haag, S. T.; Hofacker, L.; Kappel, C.; Strunk, H. P.; Richter, G. The filamentary growth of metals. *International Journal of Materials Research* **2011**, *102* (7), 828−836.

(24) Escobar Galindo, R.; Manninen, N. K.; Palacio, C.; Carvalho, S. Advanced surface characterization of silver nanocluster segregation in Ag−TiCN bioactive coatings by RBS, GDOES, and ARXPS. *Anal. Bioanal. Chem.* **2013**, *405* (19), 6259−6269.

(25) Shao, W.; Zhang, X.; Jiang, B.; Liu, C.; Li, H. Spontaneous escape behavior of silver from graphite-like carbon coating and its inhibition mechanism. *Journal of Materials Science & Technology* **2017**, *33* (11), 1402−1408.

(26) Wang, L. J.; Zhang, F.; Fong, A.; Lai, K. M.; Shum, P. W.; Zhou, Z. F.; Gao, Z. F.; Fu, T. Effects of silver segregation on sputter deposited antibacterial silver-containing diamond-like carbon films. *Thin Solid Films* **2018**, *650*, 58−64.

(27) Carvalho, I.; Curado, M.; Palacio, C.; Carvalho, S.; Cavaleiro, A. Ag release from sputtered Ag/a:C nanocomposite films after immersion in pure water and NaCl solution. *Thin Solid Films* **2019**, *671*, 85−94.

(28) Manninen, N. K.; Galindo, R. E.; Carvalho, S.; Cavaleiro, A. Silver surface segregation in Ag-DLC nanocomposite coatings. *Surf. Coat. Technol.* **2015**, *267*, 90−97.

(29) Agnihotri, S.; Mukherji, S.; Mukherji, S. Size-controlled silver nanoparticles synthesized over the range 5−100 nm using the same protocol and their antibacterial efficacy. *RSC Adv.* **2014**, *4* (8), 3974−3983.

(30) Zhang, W.; Yao, Y.; Sullivan, N.; Chen, Y. Modeling the Primary Size Effects of Citrate-Coated Silver Nanoparticles on Their Ion Release Kinetics. *Environ. Sci. Technol.* **2011**, *45* (10), 4422.

(31) Xiu, Z.-M.; Zhang, Q.-B.; Puppala, H. L.; Colvin, V. L.; Alvarez, P. J. Negligible Particle-Specific Antibacterial Activity of Silver Nanoparticles. *Nano Lett.* **2012**, *12* (8), 4271−4275.

(32) Zhao, Y.; Zhang, Z.; Pan, Z.; Liu, Y. Advanced bioactive nanomaterials for biomedical applications. *Exploration* **2021**, *1* (3), 20210089.

(33) Shao, W.; Jiang, B.; Ma, J.; Yan, F. Mechanism for vacuum thermal stabilization of silver in graphite-like carbon coating and performance of electrical conductivity and corrosion resistance. *Thin Solid Films* **2020**, *693*, 137658.

(34) de los Arcos, T.; Oelhafen, P.; Aebi, U.; Hefti, A.; Düggelin, M.; Mathys, D.; Guggenheim, R. Preparation and characterization of TiN−Ag nanocomposite films. *Vacuum* **2002**, *67* (3), 463−470.

(35) Mulligan, C. P.; Blanchet, T. A.; Gall, D. CrN−Ag nanocomposite coatings: High-temperature tribological response. *Wear* **2010**, *269* (1), 125−131.

(36) Mulligan, C. P.; Papi, P. A.; Gall, D. Ag transport in CrN−Ag nanocomposite coatings. *Thin Solid Films* **2012**, *520* (22), 6774−6779.

(37) Manninen, N. K.; Figueiredo, N. M.; Carvalho, S.; Cavaleiro, A. Production and Characterization of Ag Nanoclusters Produced by Plasma Gas Condensation. *Plasma Processes and Polymers* **2014**, *11* (7), 629−638.

(38) Kousal, J.; Shelemin, A.; Schwartzkopf, M.; Polonskyi, O.; Hanuš, J.; Solař, P.; Vaidulych, M.; Nikitin, D.; Pleskunov, P.; Krtouš, Z.; Strunskus, T.; Faupel, F.; Roth, S.; Biederman, H.; Choukourov, A. Magnetron-sputtered copper nanoparticles: lost in gas aggregation and found by in situ X-ray scattering. *Nanoscale* **2018**, *10* (38), 18275−18281.

(39) Mattei, J.-G.; Grammatikopoulos, P.; Zhao, J.; Singh, V.; Vernieres, J.; Steinhauer, S.; Porkovich, A.; Danielson, E.; Nordlund, K.; Djurabekova, F.; Sowwan, M. Gas-Phase Synthesis of Trimetallic Nanoparticles. *Chem. Mater.* **2019**, *31* (6), 2151−2163.

(40) Cavaliere, E.; Benetti, G.; Banfi, F.; Gavioli, L. Antimicrobial nanostructured coating. In *Cluster Beam Deposition of Functional Nanomaterials and Devices*; Milani, P., Sowwan, M., Eds.; Elsevier, 2020; Chapter 11, Vol. *15*, pp 291−311.

(41) Sanzone, G.; Yin, J.; Cooke, K.; Sun, H.; Lievens, P. Impact of the gas dynamics on the cluster flux in a magnetron cluster-source: Influence of the chamber shape and gas-inlet position. *Rev. Sci. Instrum.* **2021**, *92* (3), 033901.

(42) Charitidis, C. A. Nanomechanical and nanotribological properties of carbon-based thin films: A review. *International Journal of Refractory Metals and Hard Materials* **2010**, *28* (1), 51−70.

(43) Jarratt, M.; Stallard, J.; Renevier, N. M.; Teer, D. G. An improved diamond-like carbon coating with exceptional wear properties. *Diamond Relat. Mater.* **2003**, *12* (3), 1003−1007.

(44) Grimanelis, D.; Yang, S.; Böhme, O.; Román, E.; Alberdi, A.; Teer, D. G.; Albella, J. M. Carbon based coatings for high temperature cutting tool applications. *Diamond Relat. Mater.* **2002**, *11* (2), 176−184.

(45) Amaro, R.I.; Martins, R.C.; Seabra, J.O.; Yang, S.; Teer, D.G.; Renevier, N.M. Carbon/chromium low friction surface coating for gears application. *Industrial Lubrication and Tribology* **2005**, *57* (6), 233−242.

(46) Yari, M.; Larijani, M. M.; Afshar, A.; Eshghabadi, M.; Shokouhy, A. Physical properties of sputtered amorphous carbon coating. *J. Alloys Compd.* **2012**, *513*, 135−138.

(47) Dai, H. Y.; Cheng, X. R.; Wang, C. F.; Xue, Y. C.; Chen, Z. P. Structural, optical and electrical properties of amorphous carbon films deposited by pulsed unbalanced magnetron sputtering. *Optik* **2015**, *126* (7), 861−864.

(48) Yang, S.; Camino, D.; Jones, A. H.; Teer, D. G. Deposition and tribological behaviour of sputtered carbon hard coatings. *Surf. Coat. Technol.* **2000**, *124* (2), 110−116.

(49) Yang, S.; Li, X.; Renevier, N. M.; Teer, D. G. Tribological properties and wear mechanism of sputtered C/Cr coating. *Surf. Coat. Technol.* **2001**, *142−144*, 85−93.

(50) Kashtanov, P. V.; Smirnov, B. M.; Hippler, R. Magnetron plasma and nanotechnology. *Physics-Uspekhi* **2007**, *50* (5), 455−488.

(51) Grammatikopoulos, P.; Sowwan, M.; Kioseoglou, J. Computational Modeling of Nanoparticle Coalescence. *Advanced Theory and Simulations* **2019**, *2* (6), 1900013.

(52) Ganeva, M.; Peter, T.; Bornholdt, S.; Kersten, H.; Strunskus, T.; Zaporojtchenko, V.; Faupel, F.; Hippler, R. Mass Spectrometric Investigations of Nano-Size Cluster Ions Produced by High Pressure Magnetron Sputtering. *Contributions to Plasma Physics* **2012**, *52* (10), 881−889.

(53) Sanna, G.; Tomassetti, G. *Introduction to molecular beams gas dynamics*; Imperial College Press: London, 2005.

(54) Sanzone, G.; Yin, J.; Sun, H. Scaling up of cluster beam deposition technology for catalysis application. *Frontiers of Chemical Science and Engineering* **2021**, *15* (6), 1360−1379.

(55) Erdemir, A.; Donnet, C. Tribology of diamond-like carbon films: recent progress and future prospects. *J. Phys. D: Appl. Phys.* **2006**, *39* (18), R311−R327.

(56) Bewilogua, K.; Hofmann, D. History of diamond-like carbon films — From first experiments to worldwide applications. *Surf. Coat. Technol.* **2014**, *242*, 214−225.

(57) Bloyce, A. Surface engineering in motorsport for improved tribological performance. *Surface Engineering* **2010**, *26* (1−2), 55−60.

(58) Mangolini, F.; Krick, B. A.; Jacobs, T. D. B.; Khanal, S. R.; Streller, F.; McClimon, J. B.; Hilbert, J.; Prasad, S. V.; Scharf, T. W.; Ohlhausen, J. A.; Lukes, J. R.; Sawyer, W. G.; Carpick, R. W. Effect of silicon and oxygen dopants on the stability of hydrogenated amorphous carbon under harsh environmental conditions. *Carbon* **2018**, *130*, 127−136.

(59) Field, S. K.; Jarratt, M.; Teer, D. G. Tribological properties of graphite-like and diamond-like carbon coatings. *Tribiol. Int.* **2004**, *37* (11−12), 949−956.

(60) Taga, Y.; Takahasi, R. Role of kinetic energy of sputtered particles in thin film formation. *Surf. Sci.* **1997**, *386* (1), 231−240.

(61) Alvarez, R.; Garcia-Valenzuela, A.; Rico, V.; Garcia-Martin, J. M.; Cotrino, J.; Gonzalez-Elipe, A. R.; Palmero, A. Kinetic energy-induced growth regimes of nanocolumnar Ti thin films deposited by evaporation and magnetron sputtering. *Nanotechnology* **2019**, *30* (47), 475603.

(62) Choi, H. W.; Choi, J.-H.; Lee, K.-R.; Ahn, J.-P.; Oh, K. H. Structure and mechanical properties of Ag-incorporated DLC films prepared by a hybrid ion beam deposition system. *Thin Solid Films* **2007**, *516* (2), 248−251.

(63) Matenoglou, G.; Evangelakis, G. A.; Kosmidis, C.; Foulias, S.; Papadimitriou, D.; Patsalas, P. Pulsed laser deposition of amorphous carbon/silver nanocomposites. *Appl. Surf. Sci.* **2007**, *253* (19), 8155−8159.

(64) Haberland, H. History, Some Basics, and an Outlook. In *Gas-Phase Synthesis of Nanoparticles*; Huttel, Y., Ed.; Wiley-VCH: Weinheim Germany, 2017; Chapter 1, p 9.

(65) Dai, W.; Wang, A.; Wang, Q. Microstructure and mechanical property of diamond-like carbon films with ductile copper incorporation. *Surf. Coat. Technol.* **2015**, *272*, 33−38.

(66) Chen, C.-C.; Hong, F. C.-N. Structure and properties of diamond-like carbon nanocomposite films containing copper nanoparticles. *Appl. Surf. Sci.* **2005**, *242* (3), 261−269.

(67) Hrkac, T.; Röhl, C.; Podschun, R.; Zaporojtchenko, V.; Strunskus, T.; Papavlassopoulos, H.; Garbe-Schönberg, D.; Faupel, F. Huge increase of therapeutic window at a bioactive silver/titania nanocomposite coating surface compared to solution. *Materials Science and Engineering: C* **2013**, *33* (4), 2367−2375.

(68) Sotiriou, G. A.; Teleki, A.; Camenzind, A.; Krumeich, F.; Meyer, A.; Panke, S.; Pratsinis, S. E. Nanosilver on nanostructured silica: Antibacterial activity and Ag surface area. *Chemical Engineering Journal* **2011**, *170* (2), 547−554.

(69) Senatore, G.; Mastroleo, F.; Leys, N.; Mauriello, G. Effect of microgravity & space radiation on microbes. *Future Microbiology* **2018**, *13* (7), 831−847.

(70) Zea, L.; Larsen, M.; Estante, F.; Qvortrup, K.; Moeller, R.; Dias de Oliveira, S.; Stodieck, L.; Klaus, D. Phenotypic Changes Exhibited by E. coli Cultured in Space. *Frontiers in Microbiology* **2017**, *8*, 1598.